ACS APPLIED MATERIALS & INTERFACES

www.acsami.org Research Article

Ultrasmall AgNP-Impregnated Biocompatible Hydrogel with Highly Effective Biofilm Elimination Properties

Hanif Haidari, Zlatko Kopecki, Richard Bright, Allison J. Cowin, Sanjay Garg, Nirmal Goswami,* and Krasimir Vasilev*

Cite This: https://dx.doi.org/10.1021/acsami.0c09414 Read Online

ACCESS | Metrics & More | Article Recommendations | Supporting Information

ABSTRACT: Ultrasmall silver nanoparticles (AgNPs; size < 3 nm) have attracted a great deal of interest as an alternative to commercially available antibiotics due to their ability to eliminate a wide range of microbial pathogens. However, most of these ultrasmall AgNPs are highly reactive and unstable, as well as susceptible to fast oxidation. Therefore, both the stability and toxicity remain major shortcomings for their clinical application and uptake. To circumvent these problems, we present a novel strategy to impregnate ultrasmall AgNPs into a biocompatible thermosensitive hydrogel that enables controlled release of silver alongside long-term storage stability and highly potent antibacterial activity. The advantage of this strategy lies in the combination of a homogenous dispersion of AgNPs in a hydrogel network, which serves as a sustained-release reservoir, and the unique feature of ultrasmall AgNP size, which provides an improved biofilm eradication capacity. The superior biofilm dispersion properties of the AgNP hydrogel is demonstrated in both single-species and multispecies biofilms, eradicating ~80% of established biofilms compared to untreated controls. Notably, the effective antibacterial concentration of the formulation shows minimal toxicity to human fibroblasts and keratinocytes. These findings present a promising novel strategy for the development of AgNP hydrogels as an efficient antibacterial platform to combat resistant bacterial biofilms associated with wound infections.

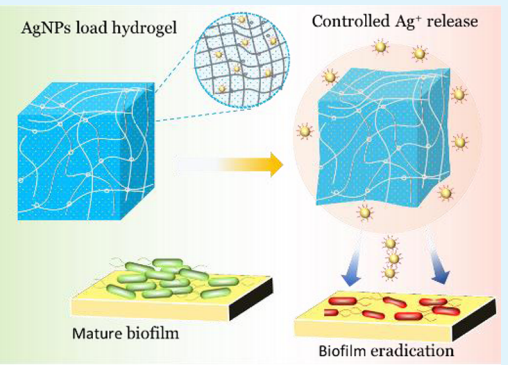

KEYWORDS: *ultrasmall silver nanoparticles, hydrogel, antibacterial nanoparticles, topical delivery of silver nanoparticles, multispecies biofilm disruption*

INTRODUCTION

The rise in antibiotic resistance is becoming a major health threat globally, which accounts for the deaths of 23 000 people annually in the United States alone. The estimated global human death toll is expected to be 10 million by 2050 as a direct result of antibiotic-resistant infection.[1−3] Persistent bacterial wound infections are mediated by highly organized structures known as biofilms, which are communities of bacteria and extracellular matrix where individual cells have close interactions and produce a protective substrate to which they adhere.[4] Unlike bacteria in a planktonic state, biofilms present many challenges, predominately due to their inherent resistance to both antimicrobials and natural host defenses.[5,6] The rapid emergence of drug-resistant bacterial infections and the challenges associated with the treatment of biofilms highlight the demand for alternative antimicrobial agents that provide effective solutions against this clinical problem.

Current antimicrobial strategies include the use of antibiofilm coatings, which are effective in eliminating both single- and multispecies bacterial cultures.[7−9] However, a substantial challenge is presented when bacteria become encased in protective polymeric substances and form biofilms. These biofilms tend to become resistant to many of the traditionally used antibiotics due to alterations in phenotype, their acquisition of a physical barrier, and extended bacterial life cycles.[10,11]

Local wound infections that resist treatment by traditional antibiotic strategies are susceptible to transform into severe chronic infections and systemic sepsis resulting in serious health consequences. In most cases, chronic wound biofilms are very complex and consist of multispecies pathogens.[12] This leads to challenging consequences including increased biofilm biomass and elevated resistance to antimicrobial agents as well as greater bacterial pathogenicity.[13,14] For example, a significant increase in antibiotic tolerance in multispecies biofilms was observed *in vitro*, which leads to longer treatments with higher drug concentrations, which in turn further contributed to the development of antibiotic resistance.[15]

Received: May 23, 2020
Accepted: August 25, 2020
Published: August 25, 2020

https://dx.doi.org/10.1021/acsami.0c09414
ACS Appl. Mater. Interfaces XXXX, XXX, XXX−XXX

Scheme 1. Schematic Illustration of AgNPs@MSA-Loaded Pluronic Hydrogel Preparation

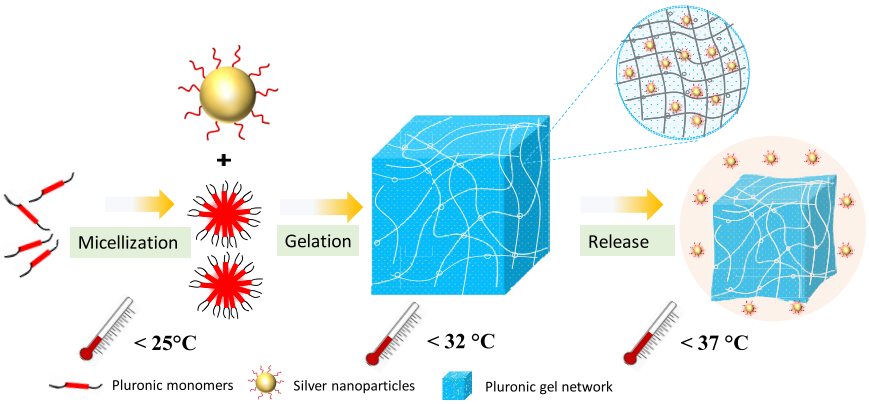

As traditional commercial antimicrobials have failed to mitigate the threat of antibiotic resistance, other materials, including silver nanoparticles (AgNPs), have emerged as potential alternatives due to their broad-spectrum antimicrobial actions.[16−19] We have recently reported that mercaptosuccinic acid (MSA)-coated AgNPs (AgNPs@MSA) with size ∼3 nm show excellent antibacterial activity against bacteria in their planktonic state.[20] However, these ultrasmall AgNPs are highly susceptible to fast oxidation that leads to rapid silver ion release, resulting in an only short-term activity that limits their tractability in antimicrobial applications.[21] Additionally, when the local concentration of silver ions is high, healthy cells are also susceptible to the toxic effects of silver. Thus, the use of lower concentrations of AgNPs alongside slower release while still showing strong bactericidal activity is a desirable way to reduce unwanted cellular toxicity.

The goal of this study was to overcome the current shortfalls of silver as an antimicrobial agent by incorporating AgNPs in a hydrogel to provide a controlled and localized delivery platform (Scheme 1). This strategy would enable the delivery of AgNPs at the target site (e.g., an infected wound) and in an adequate concentration to eliminate bacterial pathogen colonization without toxic side effects to mammalian cells. Another, even more ambitious goal was to eliminate established biofilms. We hypothesized that the ultrasmall size of the AgNPs would penetrate the dense extracellular matrix of bacterial biofilms, hence facilitating enhanced killing and elimination of the pathogens. Lastly, the hydrogel formulation would be safe and nontoxic to mammalian cells in a wound environment, which is a critical requirement for biomedical devices in these clinical settings.

Pluronic F-127 polymer was utilized as a carrier for the AgNPs as this triblock copolymer possesses excellent thermoreversible properties in aqueous solution. Also, it is generating growing interest as a carrier for nanomaterials due to its excellent solubility and stability.[22] Furthermore, Pluronic F-127 is both biocompatible and Food and Drug Administration (FDA)-approved, which is important for the development of antibacterial platforms for the treatment of infected wounds.[23−26]

The antibacterial performance of the delivery system was investigated against both Gram-negative and Gram-positive bacteria in both planktonic and biofilm states, including multispecies biofilms. The safety of the AgNP formulation was evaluated against human keratinocytes and fibroblasts to ensure a lack of toxicity and a high degree of biocompatibility. The development of this nanocomposite offers new hope to elucidate drug resistance and improve wound-infection-related treatment outcomes in clinical settings.

EXPERIMENTAL SECTION

Materials. $AgNO_3$ (99.99%), mercaptosuccinic acid (MSA), sodium borohydride ($NaBH_4$), Pluronic F-127, propylene glycol (PG), resazurin sodium salt, 2′,7′-dichlorofluorescin diacetate (DCFH-DA), nitric acid (HNO_3), sodium hydroxide (NaOH), and hexamethyldisilazane (HMDS) were purchased from Sigma-Aldrich (Sydney, Australia). All other reagents used throughout the study were of analytical grade, commercially available, and used without further purifications. Ultrapure water with 18.2 MΩ (Millipore) was used in all syntheses and preparations.

Synthesis of MSA-Coated AgNPs. For the preparation of the MSA-coated AgNPs, 1 mL of 20 mM $AgNO_3$ and 1 mL of 20 mM MSA were first mixed in 7.7 mL of MilliQ water under vigorous stirring (ice-cold condition) to form Ag(I)−thiolate complexes. After a 5 min stirring, 0.3 mL of 0.05 M $NaBH_4$ (prepared in 20% 1 M NaOH) was introduced to the reaction mixture. Subsequently, the reaction was stirred at 500 rpm for 24 h. The slow progress of color change from pale to bright yellow confirmed the formation of AgNPs@MSA. After the synthesis, the NP solution was purified through dialysis (Pur-A-Lyzer Maxi Dialysis Kit; MWCO 3.5 kDa) against ultrapure water, lyophilized using Modulyo freeze, and stored for further use. Under the same synthesis conditions, the scalability of AgNPs@MSA was verified for up to 250 mL of total solution.

Preparation of Pluronic Hydrogel. The Pluronic F-127 hydrogel base was prepared based on the cold method described previously.[27] The hydrogel was prepared by adding the preweighed quantity of Pluronic F-127 and Propylene glycol slowly to MilliQ water with or without AgNPs, keeping the system in a cold bath. The resulting formulation was transferred to the refrigerator at 4 °C overnight to ensure the complete dissolution of PF-127.

Characterization of AgNPs. The optical properties of the purified AgNP solution were characterized using UV−vis spectroscopy (Shimadzu 2600, Japan). The optical properties of AgNPs in the formulation were determined by diluting the hydrogel in 1:3 with MilliQ water. Dynamic light scattering (DLS) (Malvern Zetasizer Nano) was used to measure the hydrodynamic diameter and ζ-potential of the samples. The primary size and morphology of AgNPs were determined by transmission electron microscopy (TEM) (JEOL 3010) operating at 200 kV. The AgNP size distribution was determined by counting over 250 nanoparticles using ImageJ software (Fiji).

Characterization and Evaluation of Thermosensitive Hydrogel. The silver concentration in the hydrogel was verified using inductively coupled optical emission spectroscopy (ICP-OES). For this, 1 mL of the gel formulation was dissolved in 4 mL of HNO_3 (70% v/v) and it was brought to a volume of 10 mL with MilliQ

https://dx.doi.org/10.1021/acsami.0c09414
ACS Appl. Mater. Interfaces XXXX, XXX, XXX−XXX

water. The resulting solution was filtered (0.25 μm), and the silver concentration (atomic) was analyzed using ICP-OES.

AgNP Formulation Stability. The effect of short-term storage condition on AgNP formulation and AgNP solution was studied at three different storage temperatures (fridge 4 °C, room temperature 25 °C, and incubator 37 °C) covered with an aluminum foil. At different time intervals of 0, 7, 30, and 60 days, a representative batch was withdrawn and subjected to UV−vis, DLS, and ζ-potential measurements. AgNPs were monitored over time based on their chemical and physical properties at different temperature conditions.

Rheological Properties. The rheological experiments were carried out on a rheometer (TA instrument) using a parallel plate with a diameter of 25 mm. The oscillatory shear rate sweep was carried out at a constant temperature of 25 °C and a shear rate of 1−200 s^{-1}. Additionally, rate sweep measurements were also conducted to determine the hydrogel viscosity. The temperature analysis of the hydrogel was measured using a single frequency strain-controlled temperature ramp from 20 to 40 °C at constant shear stress (0) and strain of 1% to acquire the storage modulus (G') and loss modulus (G'') with respect to temperature.

Thermogravimetric Analysis (TGA). Thermal analysis of the blank hydrogel and the silver hydrogel was measured using TGA (TA instruments Discovery). Approximately 5 mg of sample was placed in an open pan (platinum) attached to a microbalance. The samples were heated at 20 °C/min from 25 to 700 °C under dry nitrogen with a flow rate of 10 mL/min in the standard mode with a ramp test type. All of the measurements were performed in duplicate.

Scanning Electron Microscopy (SEM). The microstructure of the hydrogel was examined using scanning electron microscopy (SEM) (Zeiss Merlin FEG). The swollen hydrogel samples were transferred to liquid nitrogen and then freeze-dried under vacuum for 24 h or until completely dry. The dried hydrogels were mounted on SEM stubs and sputter-coated with platinum and then imaged using a scanning electron microscope at 2 kV at different magnifications (10× and 30×). The composition of major elements present on the surface of the AgNP hydrogel was analyzed using energy-dispersive X-ray spectrometer (EDS) mapping at an acceleration voltage of 15 kV (SEM Zeiss Merlin FEG with SDD EDS).

***In Vitro* Release Study.** The *in vitro* release of AgNPs from the prepared hydrogel formulations was studied using a dialysis membrane approach. Dialysis (12 kDa CelluSep Western Australia) was presoaked in MilliQ water for 1 h prior to the experiment and then rinsed with water to remove preservatives. Two milliliter samples of the formulation were dispensed into the dialysis membrane as a donor compartment. The bag was firmly tied and immersed into a 50 mL falcon tube (receptor compartment) containing 10 mL of phosphate-buffered saline (PBS) pH 7.4 as the release medium. The system was maintained at 37 ± 0.5 °C in a thermostatically controlled shaking incubator at ∼85 rpm. Aliquots of 2 mL were withdrawn at intervals of 0.5, 1, 2, 3, 4, 6, 8, 10, and 24 h, which were replaced by the same volume of fresh solution (kept at the same temperature) to maintain a constant volume. The collected solution was diluted accordingly to be analyzed by ICP-OES. The experiment was conducted using two replicates on three different occasions.

***In Vitro* Antibacterial Evaluation of AgNPs.** *Bacterial Strains and Culture.* *Staphylococcus epidermidis* ATCC 35984, *Staphylococcus aureus* ATCC 25923, *Escherichia coli* 10P50, and *Pseudomonas aeruginosa* PAO1 were streaked on Mueller Hinton Agar (MHA) plates. Bacterial cultures were prepared by isolating a single colony and suspending it in 10 mL of sterile tryptic soy broth (TSB) medium incubated overnight (16−18 h) at 37 °C in a shaking incubator. The optical density was measured at 660_{nm} (OD 660) and standardized by diluting the overnight culture to 0.25, which equates to approximately 2.5 × 10^8 colony-forming units (CFU)/mL. The resulting standardized inoculum was further diluted as required.

Well Diffusion Assay. Overnight culture of bacterial strains was adjusted to OD 660_{nm} 0.25 and diluted further to obtain 1 × 10^6 CFU/mL. The bacterial lawn was prepared by adding 100 μL of diluted inoculum onto the diagnostic sensitivity test agar surface (Oxoid) and spread uniformly. A well with a diameter of 6 mm was punched aseptically with a sterile cork borer, and a volume of 100 μL of the formulation and positive control (ciprofloxacin) and negative controls (TSB) were introduced into the well. The agar plates were incubated at 37 °C overnight (16−18 h), and the zone of inhibition (mm) was measured the following day.

Live/Dead Viability Assay. The bacterial viability was quantitatively evaluated using the Live/Dead Baclight viability kit as per the manufacturer's manual (Invitrogen, Thermo Fisher Scientific). An overnight culture of bacteria was cultured in TSB at 37 °C and then diluted to 1 × 10^6 CFU/mL in fresh TSB. Aliquots of the bacterial suspension were grown on a sterile glass coverslip and treated with extracts of the test formulation hydrogel (25 μg/g, 50 μg/g, and blank at final concentrations) and 50 μg/mL ciprofloxacin as the positive control and the negative control. The extracts of the silver hydrogel were prepared by incubating the pure silver formulation (100 μg/g, 50 μg/g, and blank gel) in TSB (1:1) for 24 h at a 37 °C incubator. After overnight incubation at 37 °C, the wells were gently washed with PBS to remove unadhered bacteria. Then, the bacterial cells were stained with a working concentration (1:1) of 3 μL/mL PBS of SYTO9 and propidium iodide. The samples were incubated in the dark for 15 min at 25 °C, followed by a PBS wash. The glass coverslips were mounted on a microscope slide to be imaged via an Olympus FV3000 confocal laser scanning microscope (CLSM). The number of live and dead cells was quantified using ImageJ software (Fiji)1.52a.

In Vitro Biofilm Formation Assay (Crystal Violet). Sterile polystyrene flat-bottom 96-well plates were inoculated individually with standardized *S. epidermidis*, *P. aeruginosa*, and *S. aureus* suspensions at 10^6 CFU/mL. For multispecies biofilms, the individual bacteria were standardized to 10^6 CFU/mL and then combined at equal volumes (60 μL) with other bacteria to acquire a total of 180 μL of mixed bacterial population. The plates were incubated in a humid chamber for 24 h at 37 °C. After the incubation period, the planktonic bacteria were removed from each well and the wells were washed with PBS to remove any loosely attached cells. Then, 150 μL of TSB containing different concentrations of the test formulations and antibiotic control (50 μg/mL ciprofloxacin) was added to the wells and incubated for 24 h at 37 °C. The wells were washed with PBS and fixed with 10% formaldehyde for 15 min, followed by a further PBS wash. The biofilms were stained with 0.1% crystal violet (CV) for 15 min at room temperature, and the plate was washed with PBS and air-dried. The crystal violet-bound cells were solubilized with 33% acetic acid, and the released stain was measured at 550 nm using a microplate reader (ELx800 Microplate Reader, BioTek). The biofilm analysis was performed on three independent occasions.

In Vitro Wound Biofilm Model. The wound biofilm model was conducted on a permeable membrane over a semisolid agar surface that facilitates the model to resemble wound biofilms, according to Thet et al., with slight modification.[28] In brief, a polycarbonate membrane with an average pore diameter of 200 nm (Whatman) was UV-sterilized (15 min) and placed on brain heart infusion (BHI) agar. Then, the surface of the membrane was preconditioned with artificial acute wound fluid (30 μL of human serum containing 5% blood and 1% peptone) and allowed to dry. Bacterial overnight cultures of *P. aeruginosa*, *S. epidermidis*, and *S. aureus* were adjusted to OD 660_{nm} 0.25 and further diluted in 1/100 before being spotted in the center of each membrane (50 μL). After 24 h of biofilm growth at 37 °C, the membranes were aseptically transferred to new BHI agar, and biofilms were treated with 100 μL of different doses of AgNP gel (25 and 50 μg/g) and ciprofloxacin (50 μg/mL). After further 24 h of incubation, the membrane was removed, and the biofilm was stripped off from the membrane in 5 mL of PBS by a series of vigorous 2X vortexing (1 min) and 2X sonication (15 min) before being serially diluted in PBS and subjected to standard CFU counts per membrane.

Confocal Laser Scanning Microscopy (CLSM) Assessment of Biofilm Disruption. A sterile glass coverslip was placed at the bottom of 24-well plates and inoculated with 1 × 10^6 CFU/mL of *P. aeruginosa*. For multispecies biofilms, the individual bacteria were standardized to 10^6 CFU/mL and then combined at an equal volume of 60 μL with other bacteria to acquire a total of 180 μL of a mixed bacterial population. The plates were statically incubated for 24 h at

https://dx.doi.org/10.1021/acsami.0c09414
ACS Appl. Mater. Interfaces XXXX, XXX, XXX−XXX

37 °C in a humid chamber as described above. The planktonic cells were gently washed, and the biofilms were treated with 500 μL of test formulation extracts (final concentrations 25 and 50 μg/g) together with 50 μg/mL ciprofloxacin and the negative control. After a further 24 h of incubation at 37 °C, the coverslips were washed and then stained with 3 μm of SYTO9 and propidium iodide followed by 15 min in the dark at 25 °C. The excess stain was washed and mounted on a glass slide for confocal imaging. Images were visualized under CLSM and processed with Bitplane Imaris v9.0 3D/4D image analysis software.

Scanning Electron Microscopy (SEM) Analysis of Biofilm Structure. The morphology of the biofilm architecture was analyzed using SEM following established protocols.[29] The bacteria were cultured on a sterile glass coverslip for 24 h. The biofilms grown on the surface were gently washed with PBS and treated with extracts of test formulation (25 and 50 μg/g) alongside the relevant controls. Biofilms were fixed overnight with 1.25% glutaraldehyde and 4% paraformaldehyde in PBS containing 4% sucrose pH 7.4. Samples were then washed in PBS, followed by dehydration in an ascending ethanol series from 50% (v/v) to absolute ethanol. Samples were then chemically dried using hexamethyldisilazane (HMDS) and mounted on aluminum stubs, sputter-coated with 1 nm platinum, and examined in a Zeiss Merlin FEG SEM scanning electron microscope. Images were acquired using 2 kV at a working distance of ∼4 mm. Each sample was analyzed for four images at different locations and magnifications.

Measurement of Reactive Oxygen Species (ROS). To determine the generation of intracellular reactive oxygen species (ROS) as a potential cellular response to AgNPs, an ROS indicator 2,7-dichlorofluorescin-diacetate (DCFH-DA) (Sigma-Aldrich, Australia) was used. This dye is a cell-permeant, which becomes fluorescent when cleaved by intracellular esterase and oxidized by intracellular reactive species.[30] An overnight *P. aeruginosa* suspension was standardized to 10^6 CFU/mL, and 100 μL was transferred to each well of a 96-well plate for overnight growth. The cells were collected by centrifugation and washed with PBS and then incubated with 20 μm of DCFH-DA at 37 °C for 30 min in the dark. Following staining, the cells were washed and subjected to treatment of AgNP formulation extracts (25 and 50 μg/g) including positive control of 1 mM hydrogen peroxide (H_2O_2). The samples were incubated for 3 h at 37 °C in the dark, reading the fluorescence intensity every 30 min using a plate reader (Enspire PerkinElmer Multimode plate reader) with excitation at 485 nm and emission at 530 nm.

Cytotoxicity Studies. The resazurin assay was performed to determine the cell viability based on metabolically active cells as per the method described previously.[9] Briefly, human foreskin fibroblasts (HFFs) and human keratinocytes (HaCaTs) were seeded in 96-well tissue culture plates at a density of 4×10^4 cells/well in Dulbecco's modified Eagle's medium (DMEM), supplemented with 10% fetal bovine serum (FBS) and 5% penicillin and streptomycin and incubated at 37 °C in 5% CO_2 for 24 h. The cytotoxic effect of the silver formulation gel was assessed according to the previously described method using material extracts.[31] Extracts of the silver hydrogel were prepared by incubating the pure silver formulation (blank gel, 50 μg/g, and 100 μg/g) in DMEM (1:1) without FBS for 24 h at 37 °C in an incubator. After attaining approximately 90% confluency, the wells were washed with PBS and subsequently cells were treated with formulation extracts 100 μL supplemented with 10% FBS. Cells treated with fresh DMEM were used as controls. After further incubation for 24 h, the cells were washed and resazurin dye was added. The stock concentration of resazurin (110 μg/mL) was diluted 1:10 in DMEM, and the working solution was added to the wells. The cells were incubated for 2 h at 37 °C in an incubator and then the fluorescence intensity of the dye was measured using a plate reader (BMG LabTech, Australia).

Fluorescence Staining of Cell Morphology. The effect of gel extracts on HFFs and HaCaT cell morphology was determined using fluorescence staining. The existing cultured cells in 96-well plates were treated similarly as described above. The adherent cells were fixed with 3.7% formaldehyde for 10 min at room temperature, washed, and membrane-permeabilized with 0.1% Triton X-100 for 5 min before staining. The cells were stained with Phalloidin Oregano green 488 (Invitrogen, Thermo Fisher Scientific) for 20 min in the dark at a working concentration of 1:40 in PBS. The cellular nuclei were stained with diamido-2 phenyllindole dihydrochloride (DAPI) in (1:1000) PBS for 10 min. After staining, the cells were briefly washed and were imaged using an Olympus fluorescence microscope at different magnification. The images were analyzed and processed using CellSens software (Olympus Life Science, Australia) following established protocols.[32]

RESULTS AND DISCUSSION

Synthesis and Characterizations of AgNPs@MSA. The MSA-capped AgNPs were synthesized in a process similar to our previously published protocol, through a reduction decomposition reaction with slight modifications to improve size distribution and scalability.[20] Briefly, the calculated amounts of $AgNO_3$ and MSA were mixed under ice-cold conditions to form the Ag−thiol complex, followed by the addition of $NaBH_4$ to initiate reduction decomposition as depicted in the scheme in Figure 1A. The formation of

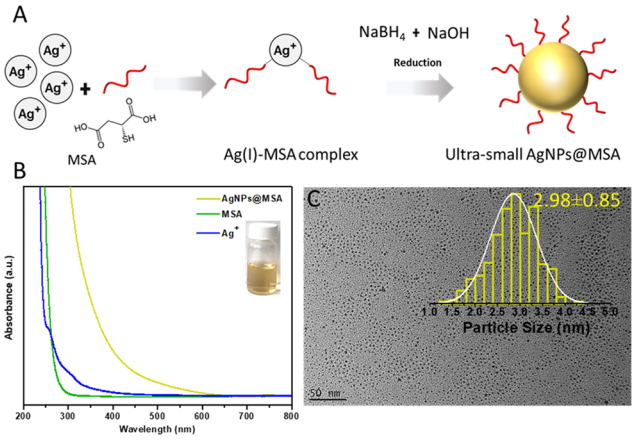

Figure 1. (A) Formation of MSA-protected AgNPs by cyclic reduction decomposition. (B) UV−vis absorption spectra of AgNPs and the controls; the inset is a representative photo of the AgNPs@MSA solution. (C) TEM micrographs of AgNPs; the inset shows the nanoparticle size distribution.

AgNPs@MSA (yellow peak) was confirmed using UV−vis spectroscopy, which shows distinct differences in the MSA (green) and Ag^+ (blue) spectra. The resultant solution was bright yellow, as shown in the inset in Figure 1B. The UV−vis spectra showed the absence of plasmon resonance absorption, which is a characteristic of ultrasmall AgNPs, consistent with previous reports.[33] The ultrasmall size of the nanoparticles was further confirmed by TEM analysis, revealing a core diameter of 2.98 ± 0.85 nm (Figure 1C). Additionally, the TEM analysis correlated well with DLS measurements (Figure S1).

Hydrogel Preparation and Characterizations. The Pluronic F-127 thermosensitive hydrogel was prepared by controlled loading of ultrasmall silver nanoparticles (AgNPs@MSA) at various concentrations (25, 50, 100, 150, and 200 μg/g). Pluronic F-127 is a well-accepted biocompatible drug carrier commonly used in topical applications. This hydrogel has known wound-healing properties that include improved cell proliferation.[34,35] Additionally, the Pluronic F-127 hydrogel also possesses thermoresponsive properties and undergoes reversible phase transitions at a lower critical solution

https://dx.doi.org/10.1021/acsami.0c09414
ACS Appl. Mater. Interfaces XXXX, XXX, XXX−XXX

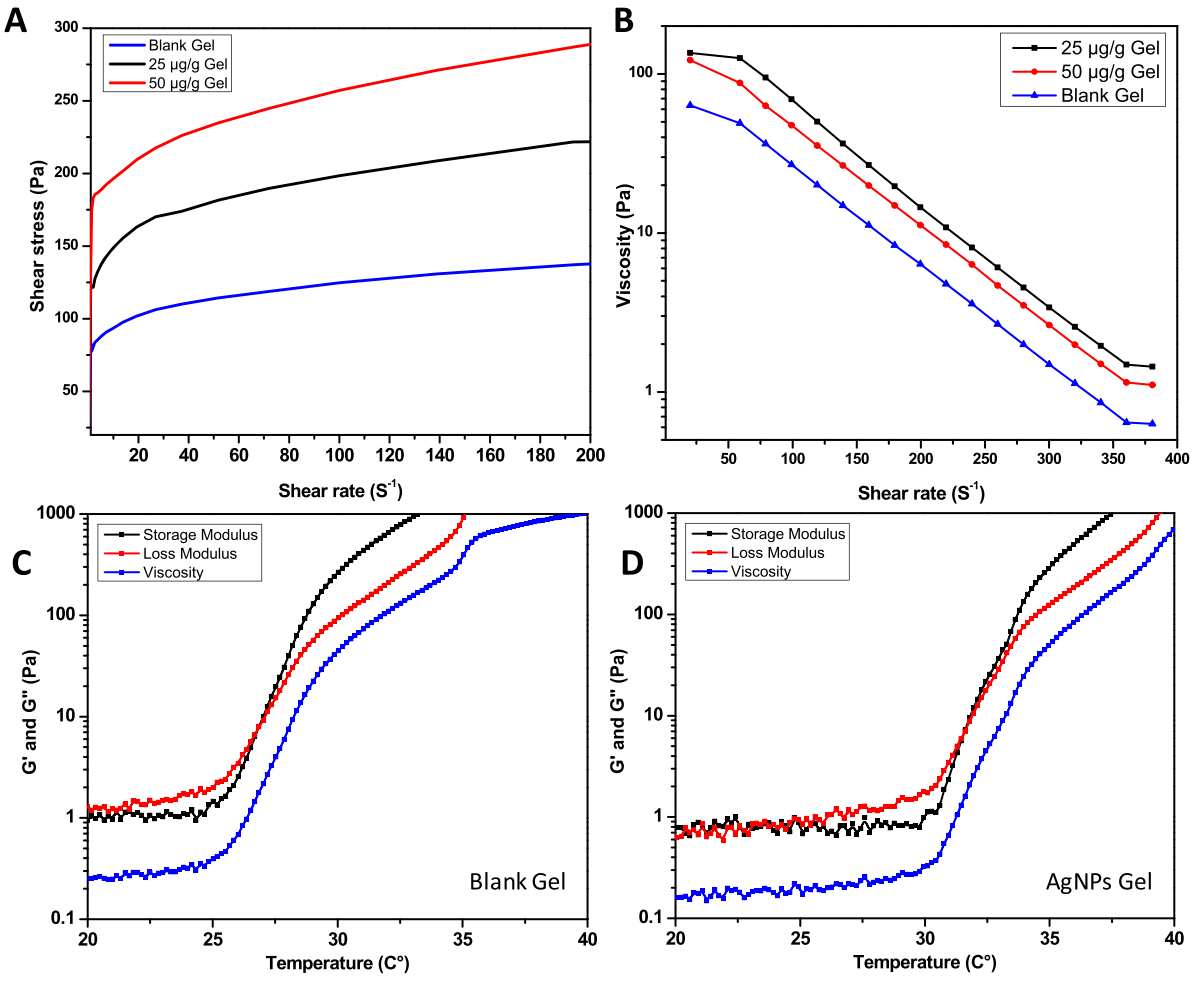

Figure 2. (A) Shear stress in response to the shear rate of the blank and the AgNP hydrogel. (B) Viscosity of the hydrogel as a function of time. (C, D) Temperature dependence of storage modulus (G') and loss modulus (G'') of the blank and the AgNP gel.

temperature (LCST).[36] Utilizing the Pluronic F-127 hydrogel has advantages including simplicity of preparation and absence of extreme conditions including heating and organic solvents, which could lead to AgNP aggregation. Changes in the AgNP surface charge and chemistry may cause the particles to become unstable and aggregate, hence resulting in changes to the intended biological activity. Following a well-rationalized preparation approach, Pluronic F-127 in combination with propylene glycol presented optimal thermoresponsive behavior (components of the hydrogel are listed in Table S1). The addition of propylene glycol was important to improve the consistency of the hydrogel as well as the development of a gel network while serving as a stabilizing emulsion. Propylene glycol modulates self-assembly of the triblock polymer due to its relative polarity to the domain structure of the gel.[37] It enhances the hydrogen bonding between water and gelling agents, thereby affecting the swelling and viscoelastic behavior of the polymeric network.[38]

Rheological Properties. The mechanical properties and solution to gel transition of the hydrogel were studied by dynamic rheology. The results of the rheological measurements are presented in Figure 2A–D. Figure 2A shows oscillatory shear rate sweeps of the Pluronic F-127 hydrogel in the presence of AgNPs, consistent with non-Newtonian fluids exhibiting shear-thinning behavior.[39] This suggests that the viscosity of the hydrogel decreases upon application of stress and there is rapid retention of its mechanical properties when the stress is reduced. Furthermore, as the shear rate increased, the viscosity reduced with no major changes observed among the blank or the AgNP hydrogel (Figure 2B). Next, the dependence of the storage modulus (G') and loss modulus (G'') was studied to determine the thermoresponsive behavior of the hydrogel. In this context, G' reflected the solidlike component dominant at a lower temperature but increased at the gelation point.[40] As shown in Figure 2C,D, the solution/gel transition temperature of the storage modulus (G') and the loss modulus (G'') of the blank gel was equal at the temperature of ∼28 °C compared to ∼34 °C for the AgNP gel. The temperature sweep measurements show that the presence of AgNPs elevated the gelation temperature. This indicates that the AgNPs may contribute to hydrogen-bonding interactions and greater cross-linking density of the hydrogel. Additionally, the transition temperature of this hydrogel is physiologically relevant to topical application in clinical use.

Hydrogel Formulation Stability. The prepared AgNP formulation was evaluated by UV–vis spectroscopy and dynamic light scattering (DLS) to monitor and determine the optimal storage condition. Given the complex nature of the hydrogel being composed of many ligands, molecules, and ions, it was critical to assess the stability of AgNPs in this environment. The results of UV–vis spectroscopy show that AgNPs loaded in the hydrogel have similar absorption spectra

https://dx.doi.org/10.1021/acsami.0c09414
ACS Appl. Mater. Interfaces XXXX, XXX, XXX–XXX

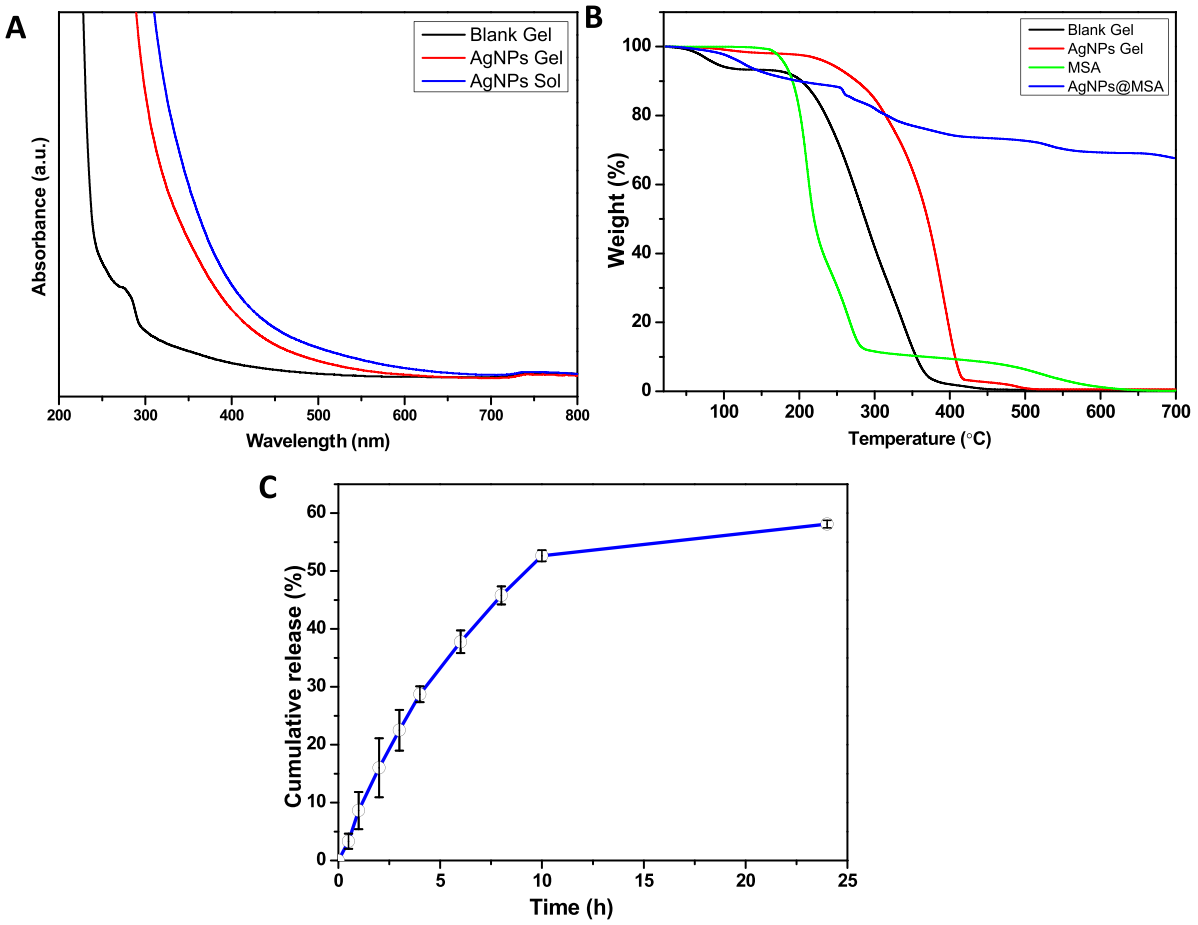

Figure 3. (A) UV−vis spectra of gels with and without AgNPs. (B) Thermogravimetric analysis of AgNP-loaded hydrogel and controls. (C) AgNP release profile from the hydrogel over a 24 h period.

f3

compared to AgNPs in solution (Figure 3A). The observed peak remained unchanged after 2 months of aging time at the storage temperatures of 4 and 25 °C, indicating the highly stable nature of the nanoparticles (Figures S1−S4). Similarly, the size of the nanoparticles remained unchanged over time as reflected by the DLS analysis at 4 and 25 °C storage on day 0 (Figure S1) and day 60 (Figure S4). The slight increase in size observed at higher temperatures (37 °C) after 2 months is expected as this condition favors the NP collision rate and subsequently induces faster agglomeration compared to the lower temperature. This was reflected in both UV−vis spectra and DLS measurements showing a slight shift in the absorption spectra and overall size distribution to the right. In contrast, at 4 and 25 °C storage, the gel displays a state of well-dispersed particles, as expected from an ideal stabilized system. The analysis of the physical state of the nanoparticles suggests that the AgNPs have maintained their native optical and physical properties after incorporation into the hydrogel network without any major alteration. More importantly, this data indicates that AgNPs@MSA are stable in the hydrogel, and Pluronic hydrogel presents a compatible carrier for silver delivery *in vivo*.

Thermogravimetric Analysis of the Hydrogel (TGA). Thermogravimetric analysis (TGA) was used to study the decomposition pattern and thermal stability of the native Pluronic hydrogel and the corresponding AgNP-loaded counterpart. The TGA spectra (Figure 3B) show the weight-loss pattern of the hydrogels and their components between 20 and 700 °C. Both hydrogels exhibited two weight-loss stages. The initial weight loss in the blank hydrogel appeared in the range of 50−130 °C, which is due to the evaporation of the adsorbed water. The major weight loss appeared in the range of 250−350 °C, which is attributed to the degradation of molecular chains.[41] However, the incorporation of AgNPs in the hydrogel improved the thermal stability, leading to a higher decomposition temperature (430 °C) and a slower thermal decomposition rate. The increased stability could be attributed to the formation of a stable hydrogen bond between the nanoparticles and the polymer and an increase in the molecular mass.[42] Additionally, the presence of AgNPs@MSA may contribute to a greater cross-linking density and subsequently a more compact structure, which may result in enhanced mechanical properties of the hydrogel. The AgNPs@MSA alone and its respective ligand shell (MSA) showed significantly different properties. The significant thermal stability of AgNPs@MSA could also be attributed to the strong thiol interaction (MSA) with the metal atoms, which results in the formation of a thermodynamically stable system. The TGA profiles for functionalized AgNPs are consistent with published studies reporting a three-stage weight loss and a significantly slower decomposition rate as previously reported.[43]

***In Vitro* Release from Pluronic Hydrogel.** The release behavior of silver from the Pluronic thermosensitive hydrogel was studied in PBS (pH 7.4) at 37 °C, which closely resembles the physiological conditions. The percentage of silver released

https://dx.doi.org/10.1021/acsami.0c09414
ACS Appl. Mater. Interfaces XXXX, XXX, XXX−XXX

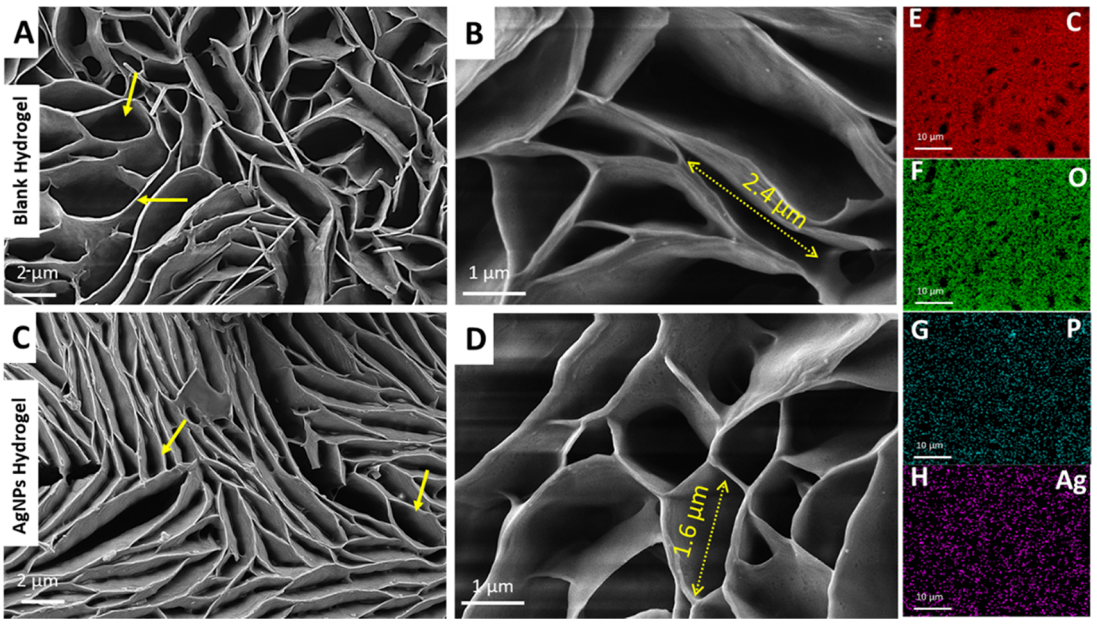

Figure 4. SEM micrograph of the blank hydrogel (A, B) and the hydrogel loaded with AgNPs (C, D) at two different magnifications. (E–H) EDS mapping of major elements present on the surface of the AgNP-loaded hydrogel.

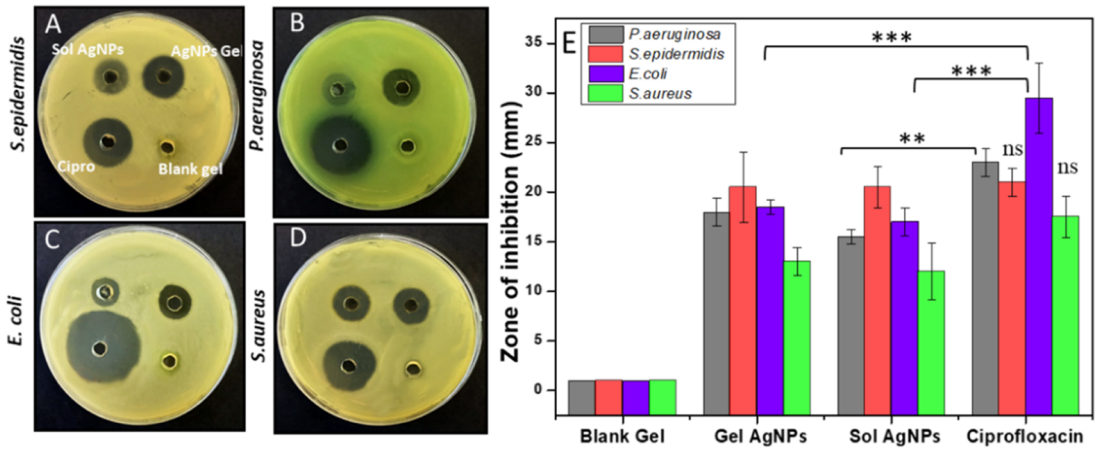

Figure 5. Antibacterial properties assessed via the disk diffusion assay. (A–D) Zone of inhibition for (A) *S. epidermidis*, (B) *P. aeruginosa*, (C) *E. coli*, and (D) *S. aureus*. (E) Quantitative measurement of the zone of inhibition (mm). Data represent the mean ± SD, and the * denotes significant difference compared to ciprofloxacin ($P < 0.05$) using one-way analysis of variance (ANOVA) followed by Tukey's multiple comparison test. *$P <$ 0.05, **$P < 0.01$, ***$P < 0.001$, and ****$P < 0.0001$.

from hydrogel formulations was plotted as a function of time and is presented in Figure 3C. The release profile is characterized by a fast release in the first 10 h when 50% of the total silver amount is released, followed by a slow continuous release for up to 24 h. This type of release profile would be beneficial for treating wound infections since it would allow for the rapid elimination of colonizing bacteria or the disruption of established biofilms. It would also provide protection of the wound from further colonization and biofilm establishment until the host immune system has recovered and is capable of eradicating the bacterial pathogens. The slow and sustained release of silver from the polymeric network is due to the combination of the slow erosion of the hydrogel and the slow diffusion of silver nanoparticles providing a synergistic release profile favoring further therapeutic development.[44]

Morphology of the Hydrogel. The interior morphology of the Pluronic hydrogel shows a relatively high porous structure in both the presence and absence of AgNPs (Figure 4A–D). The images suggest that the overall microstructure of the hydrogel is not greatly influenced by the incorporation of the AgNPs. As shown in Figure 4A–D, the interior morphology of all hydrogels demonstrated a highly three-dimensional porous structure with only slight variations in the pore diameter, labeled with the yellow arrow. The pore size was analyzed by measuring the longitudinal axis of each pore; the representative pore size is labeled with the yellow arrow. The results show that the mean pore size of the blank hydrogel is 2.01 ± 0.49 μm compared to 1.40 ± 0.4 μm for the AgNP hydrogel (Figure 4A–D). The variation in pore size could be explained by the higher cross-linking density of the AgNP-loaded hydrogel compared to the blank control hydrogel, an observation also reported for other similar systems.[44] The small change in surface morphology could be attributed to the interfacial interactions between silver nanoparticles and

https://dx.doi.org/10.1021/acsami.0c09414
ACS Appl. Mater. Interfaces XXXX, XXX, XXX–XXX

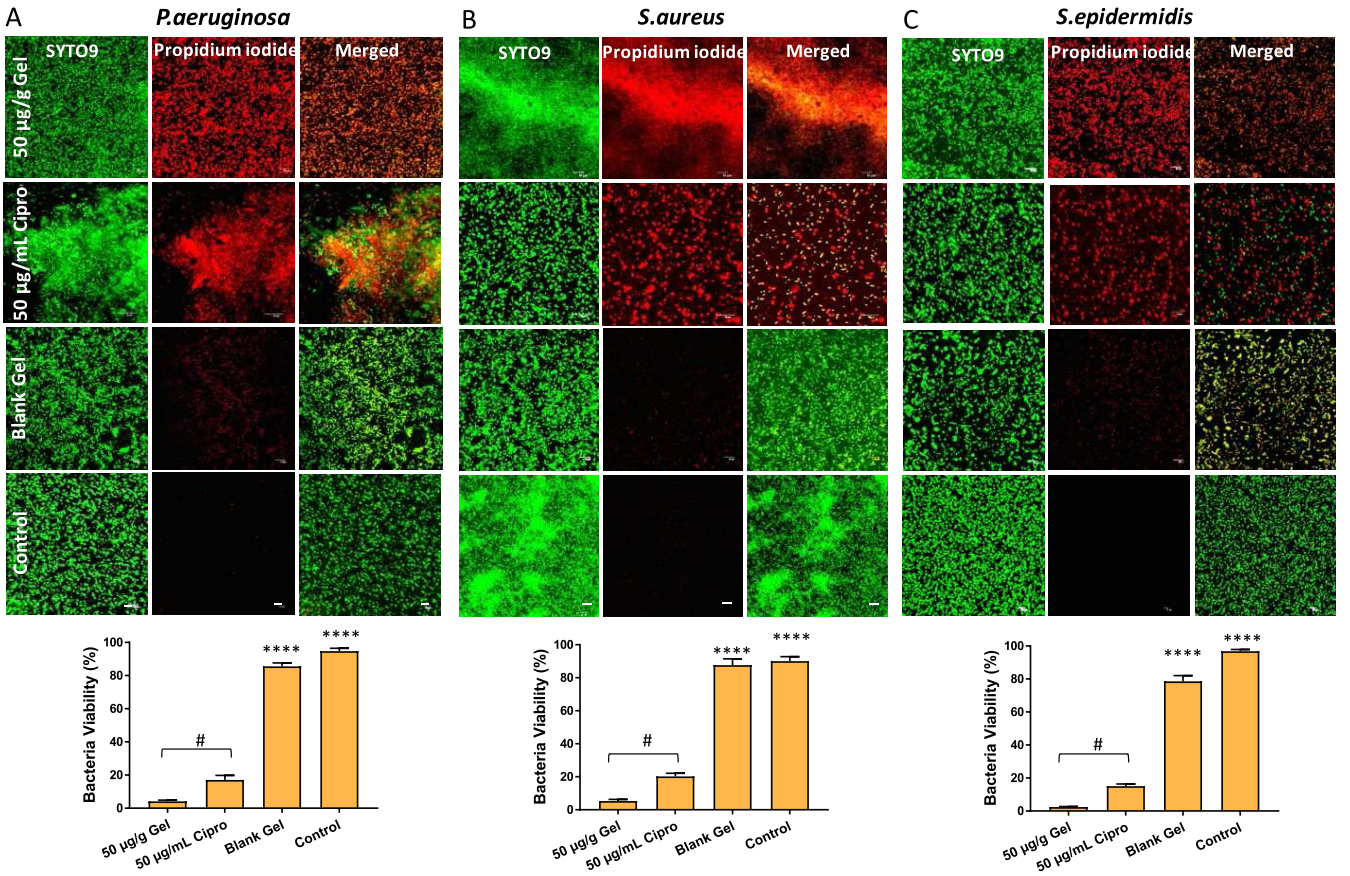

Figure 6. (A–C) Representative confocal microscopy images of Live/Dead assay of *P. aeruginosa*, *S. aureus*, and *S. epidermidis* bacteria and their corresponding quantitative analysis expressed as bacterial viability (%). Data are shown as mean ± SD; the * denotes significant difference compared to the control, and # denotes significant difference compared to ciprofloxacin ($P < 0.05$) using one-way ANOVA followed by Dunnett's multiple comparison test. $^{\#}P < 0.05$, $^{*}P < 0.05$, $^{**}P < 0.01$, $^{***}P < 0.001$, and $^{****}P < 0.0001$.

Pluronic components. The silver nanoparticle distribution in a hydrogel network was analyzed using energy-dispersive spectroscopy (EDS). The corresponding EDS micrograph confirms the presence of silver (Ag) and its homogenous distribution in the hydrogel framework (Figure 4E–H).

Antibacterial Activity of the AgNP Hydrogel. The antimicrobial performance of the AgNP hydrogel was studied against four clinically relevant pathogens including *S. epidermidis*, *S. aureus*, *E. coli*, and *P. aeruginosa*. These wound pathogens are known to pose a major health threat in the community due to the acquisition of multidrug resistance, making treatment and their eradication very challenging. The bactericidal capacities of the AgNP-loaded formulation (Gel Ag) and the AgNPs alone (Sol Ag) were first assessed using a standard well diffusion assay against *S. epidermidis*, *S. aureus*, *E. coli*, and *P. aeruginosa* (Figure 5A–E). Ciprofloxacin was used as a positive control. The results show a clear inhibition of bacterial growth by the AgNP gel and the AgNP solution, while the negative control (blank gel) did not produce a zone of inhibition (ZOI) (Figure 5A–E). The measured zone of inhibition is reported in Figure 5E. The formulation containing AgNPs had a very similar ZOI compared to the AgNP solution, demonstrating that the gel did not affect the antibacterial potency of the nanoparticles. A similar zone of inhibition was also observed when tested at lower concentrations (25 μg/g) of AgNPs (Figure S5).

The bacterial viability in response to treatment was assessed both qualitatively and quantitatively using the Live/Dead BacLight Bacterial viability kit. Bacterial cells were treated with AgNP formulation for 24 h and then stained with fluorescent dyes to determine the number of live (green) and dead (red) cells. Representative images are shown in Figure 6. Bacteria exposed to blank gels or untreated controls stain predominantly green, indicating the majority of viable cells. However, when treated with AgNP-loaded hydrogels, viability of bacterial cells significantly reduced to >97, 95, and >96% for *P. aeruginosa*, *S. aureus*, and *S. epidermidis*, respectively (Figure 6A–C). In contrast, the equal concentration of ciprofloxacin resulted in 84, 81, and 85% viability reduction for *P. aeruginosa*, *S. aureus*, and *S. epidermidis*, respectively. These results indicate that AgNPs could increase the membrane permeability of bacteria significantly, which is one of the indications of a bactericidal effect. AgNPs are known to kill bacteria by a multifaceted mechanism including binding to DNA and proteins and damaging the cell membrane.[45] We speculate that the latter plays a major role in defining the antibacterial activity of the present composition. This opinion is based on the ultrasmall size of the AgNPs and the ease of overcoming barriers to penetrate the bacterial cell membrane.

***In Vitro* Antibiofilm Assay.** The effective disruption and removal of bacterial biofilms is a significant clinical challenge as surgical debridement is not always effective and biofilms can reform quickly. Biofilms are a complex community in which the bacterial phenotype differs from that of planktonic counterparts.[46] The formation of a biofilm greatly reduces the effectiveness of antibiotics, diminishes the capacity of the

https://dx.doi.org/10.1021/acsami.0c09414
ACS Appl. Mater. Interfaces XXXX, XXX, XXX–XXX

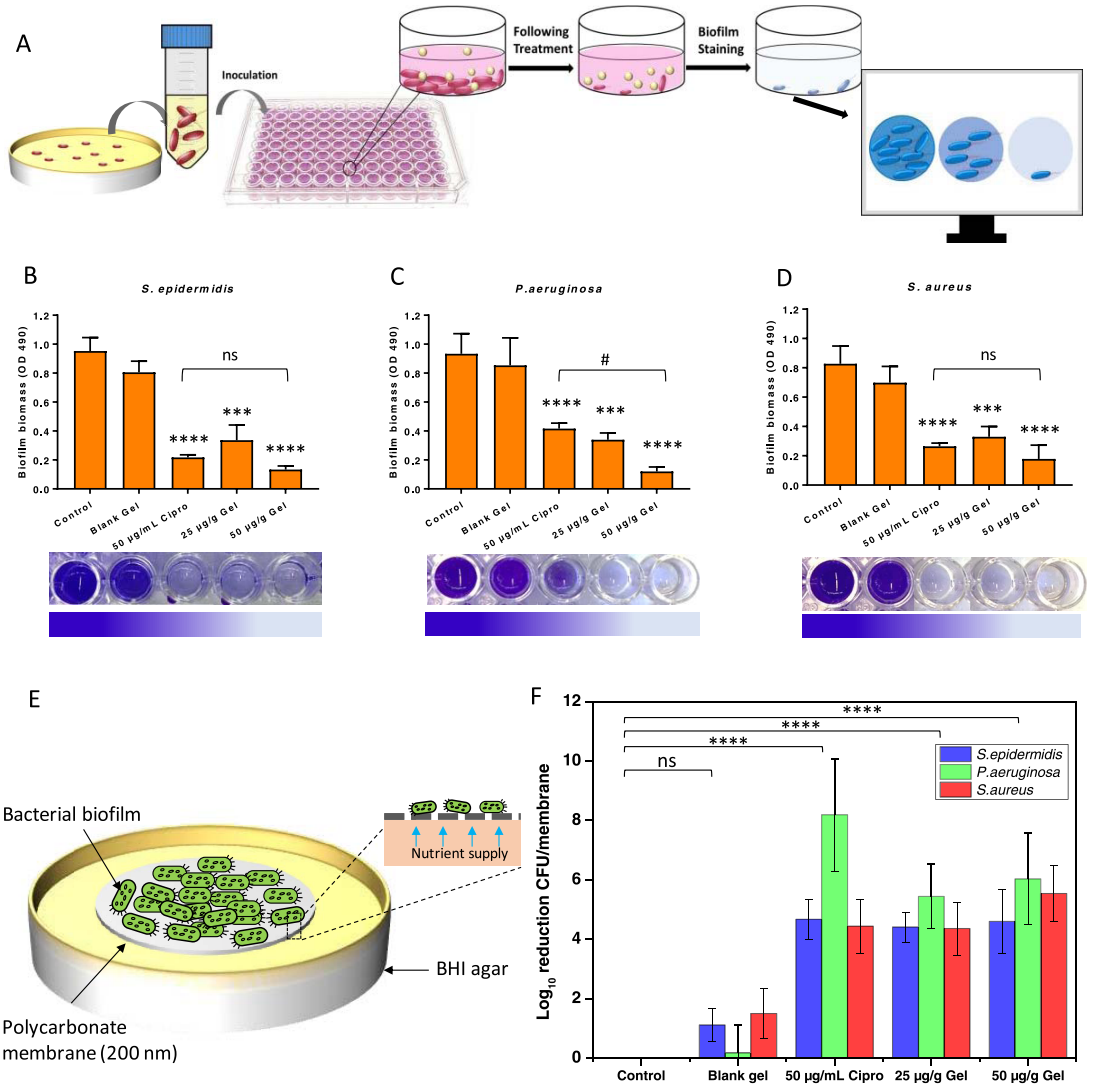

Figure 7. (A) Schematic illustration of biofilm formation and staining using crystal violet. (B–D) Eradication of single-species biofilm of *S. epidermidis*, *P. aeruginosa*, and *S. aureus* and representative images of well plates showing the intensity of crystal violet staining. (E) Schematic illustration of the colony wound biofilm model. (F) Log_{10} reduction of the bacterial biofilm colony compared to the control following treatment with AgNPs and ciprofloxacin. Data are shown as mean ± SD; the * denotes significant difference compared to the control, and # denotes significant difference compared to ciprofloxacin ($P < 0.05$) using one-way ANOVA followed by Dunnett's multiple comparison test. $^{\#}P < 0.05$, $^{*}P < 0.05$, $^{**}P < 0.01$, $^{***}P < 0.001$, and $^{****}P < 0.0001$.

immune system to fight the bacteria, and contributes to the development of antimicrobial resistance. We assessed the effectiveness of the AgNP-loaded hydrogel to disrupt and eliminate existing biofilms composed of both single and multiple clinically relevant species. For this study, bacterial biofilms were first established on a 96-well plate, treated with the AgNP formulation, and stained with crystal violet (Figure 7A). The results for a single-species biofilms of *S. epidermidis*, *S. aureus*, and *P. aeruginosa* are shown in Figure 7A–C. We found that biofilm disruption and elimination were a concentration-dependent phenomenon with 50 μg/g AgNP-loaded gel resulting in significant biofilm disruption for *S. epidermidis*, *P. aeruginosa*, and *S. aureus*. This is evident in Figure 7 and in the supporting image showing a reduction in biofilm biomass in the treated sample compared to the nontreated group. Interestingly, 50 μg/g AgNP gel showed a significantly greater antibiofilm effect than ciprofloxacin at the same concentration against *P. aeruginosa*. This finding indicates that bacterial biofilms are greatly susceptible to AgNP-loaded gels.

***In Vitro* Wound Biofilm Model.** Evaluating antibiofilm activities using *in vivo* models is challenging; hence, *in vitro* models that closely resemble a wound bed are often utilized. In this study, biofilms were grown on a nanoporous polycarbonate membrane, supplemented with artificial acute wound fluid (human serum containing 5% blood and 1% peptone). Additionally, the agar was supplemented with chopped meat-based nutrients (brain heart infusion, BHI), as well as 5% blood plasma, to replicate conditions providing ample nutrient supply to pathogens similar to conditions encountered in the clinical wound environment. A schematic representation of the wound biofilm model is shown in Figure 7E. The data are presented as a log reduction of the untreated control compared to treated groups (Figure 7F). The treatment groups had a significant reduction in the number of viable bacteria after 24 h, regardless of the bacterial strains (Figure 7F). The result showed that 25 and 50 μg/g gel had an average viable

https://dx.doi.org/10.1021/acsami.0c09414
ACS Appl. Mater. Interfaces XXXX, XXX, XXX–XXX

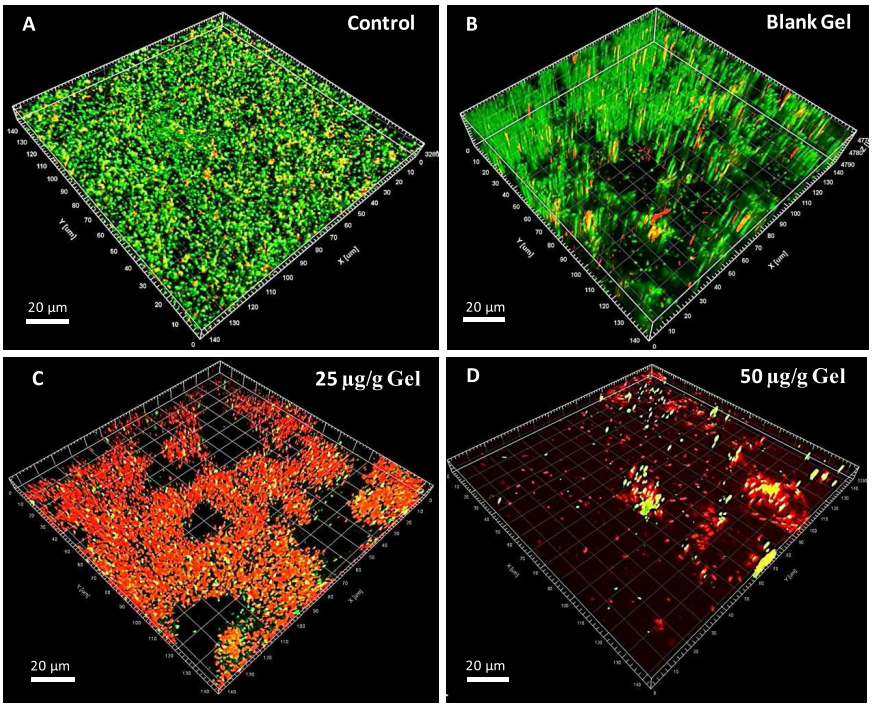

Figure 8. Three-dimensional CLSM images of the *P. aeruginosa* biofilm before (A) and after treatment with the blank gel (B) and the gel loaded with AgNPs (C, D). SYTO9 stains bacteria live (green), while propidium iodide stains bacteria dead (red).

reduction of between 4 and 5.5 $\log_{10}$ reductions compared to the untreated control across the bacterial strains. This was also comparable to ciprofloxacin at 50 μg/mL showing an average reduction of 4.5 $\log_{10}$ except for *P. aeruginosa*, which showed significantly higher susceptibility (Figure 7F). However, the blank gel was only able to reduce approx. 1.5 $\log_{10}$ bacterial reduction. These results further support the potent antibiofilm activity of AgNPs against these bacterial strains, consistent with our other *in vitro* biofilm studies. This study demonstrates the potential of the AgNP gel to eradicate established biofilms in a much more complex woundlike environment not just in standard culture plates.

Biofilm Eradication Post AgNP Treatment. To obtain further insights into the antibiofilm activity of the AgNP-loaded gel formulation, we employed confocal laser scanning microscopy (CLSM) to study the biofilm structure and eradication. In this study, *P. aeruginosa* was used because it is recognized as one of the most common bacterial species associated with persistent chronic wound infection as well as its ability to form strong adherent biofilms.[47] The confocal micrographs were taken across the depth of the biofilm to illustrate both structure thickness and bacterial cell viability. As shown in Figure 8A,B, control samples were composed of an intact thick multilayered biofilm that covered the entire surface. The Live/Dead staining showed mostly healthy cells (green staining). The result was similar when the biofilm was treated with gel, which did not contain AgNPs. In contrast, images of biofilms treated with gels containing 25 and 50 μg/g AgNPs depicted dispersed structures and extensive cell death (Figure 8C,D). In fact, when the concentration of AgNPs was increased to 50 μg/g, the majority of the biofilm biomass was detached from the surface, and the remaining colonies were killed. This observation was consistent with the crystal violet assay, demonstrating that 50 μg/g formulation was an effective concentration to eradicate established biofilms.

SEM Analysis of Bacteria Morphology. SEM imaging was used to determine morphological changes on the surface of *P. aeruginosa* cells and biofilm structure treated with the AgNP-containing gel. Visualization of bacterial biofilms with SEM showed a wide spectrum of morphological differences in the biofilm structure, as indicated with the yellow arrows (Figure 9A–D). Notably, biofilms treated with the AgNP formulation

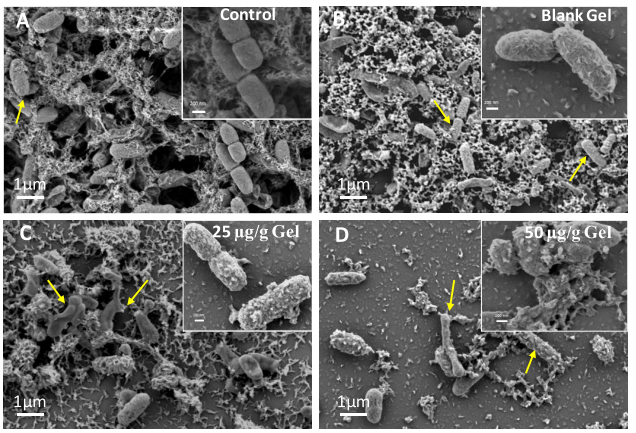

Figure 9. (A–D) Representative scanning electron microscope images of the *P. aeruginosa* biofilm structure before (A) and after treatment with the blank gel (B) and the gel loaded with AgNP formulation extracts (C, D). Inset images show the bacterial morphology at higher magnification 50 000×.

showed few scattered cell aggregates compared to the untreated biofilms, which were characterized by an intact structure connected with the extracellular matrix. The high-magnification micrographs clearly show that treated biofilms had undergone severe structural damage as the cells were ruptured, lysed, and showed clear signs of membrane blebbing.

https://dx.doi.org/10.1021/acsami.0c09414
ACS Appl. Mater. Interfaces XXXX, XXX, XXX−XXX

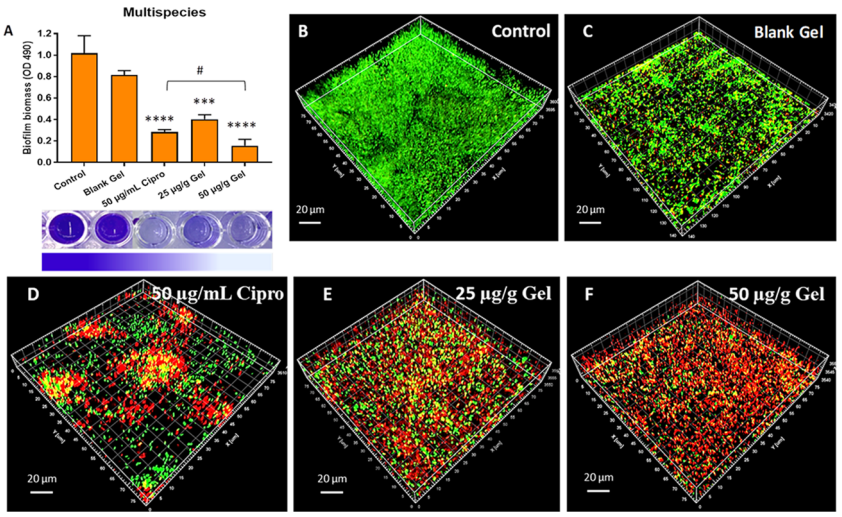

Figure 10. Three-dimensional reconstruction of the multispecies bacterial biofilm and crystal violet staining. (A) Absorbance of the crystal violet staining of biofilm biomass, (B) CLSM images of biofilm either left untreated for 24 h (B) or treated with blank gel (C), 50 μg/mL ciprofloxacin (D), and 25 and 50 μg/g AgNP gel (E, F), respectively. Data are shown as mean ±SD; the * denotes significant difference compared to the control and # denotes significant difference compared to ciprofloxacin ($P < 0.05$) using one-way ANOVA followed by Dunnett's multiple comparison test. $^{\#}P < 0.05$, $^{*}P < 0.05$, $^{**}P < 0.01$, $^{***}P < 0.001$, and $^{****}P < 0.0001$.

These pronounced changes could be attributed to the close interaction of the AgNPs and Ag ions with the bacterial membrane as well as the possible formation of reactive oxygen species.[48,49] Indeed, the application of AgNPs (50 μg/g) increased the level of intracellular reactive oxygen species by 35% in comparison to the untreated control, while the blank gel resulted only in a minimal 10% increase (Figure S6). This is consistent with previous studies showing the concentration-dependent oxidative stress following exposure of AgNPs against bacteria.[50,51] The slight increase of ROS in response to the blank is expected due to the reactivity and sensitivity of the DCHF-DA; however, this minimal increase is physiologically not relevant and unable to cause damage to the cells. However, the 35% increase in oxidative stress observed following AgNP treatment disrupts the cell membrane integrity, leading to leakage of cytoplasmic contents and ultimately bacterial cell death.[52] The excellent bactericidal activity of the gel formulation can be attributed to the small size of the AgNPs, which provides greater surface area and more contact sites for stronger and more frequent bacterial interaction. This proposed mechanism is consistent with published studies.[53] Importantly, the small AgNP size suggests possible efficient penetration to the biofilm matrix to mediate a greater degree of eradication.

Untreated biofilms were observed to be much denser and richer in the extracellular matrix. The significantly higher cell density with unaltered membrane morphology suggests a normal healthy structure, as is clearly visible at higher-magnification images (Figure 9A,B), compared to treated groups (Figure 9C,D). The SEM analysis of the biofilm corroborates well with the results of crystal violet staining and confocal image analysis presented above. The AgNP-loaded gel formulation developed in this study has a very potent antimicrobial activity and a biofilm elimination capacity that is attributed to the ultrasmall AgNP size. The gel activity is superior to many published studies and commercial antimicrobial products.[48,54] Compared to a previous study,[55] which required a significantly higher concentration of 125 μg/mL AgNPs to eliminate *P. aeruginosa* biofilms, results of the present study show significant benefits in the eradication of *P. aeruginosa* biofilms at significantly lower AgNP doses, which is clinically significant as it reduces toxicity to mammalian cells and tissue. Thus, the slower ion leaching from the hydrogel facilitates improved delivery of silver ions for enhanced activity.

Multispecies Bacterial Biofilm. The effectiveness of the developed AgNP gel against multispecies biofilms was also investigated. This is important and clinically relevant as most wound infections are composed of multiple different bacteria living in close proximity or as a biofilm. For this experiment, *S. epidermidis*, *P. aeruginosa*, and *S. aureus* were combined in equal concentrations and grown on 96-well plates for 24 h to facilitate biofilm establishment. The combination of bacteria was chosen based on their presence in typical chronic wounds and their notorious biofilm-forming capability either individually or in combinations.[56] The result indicated that the mixed bacteria formed a significantly larger biomass as determined by crystal violet staining (Figure 10A). This observation indicates that the bacteria may benefit from engagement in a mutually cooperative interaction to promote growth and pathogenicity, as previously reported.[57]

Hydrogels that contained 50 μg/g AgNPs were able to eradicate a significant amount of the established multispecies biofilm, indicating improved activity compared to an equal concentration of ciprofloxacin (Figure 10A). Additionally, the antibiofilm activities of the AgNP formulation were further examined visually using CLSM observation of biofilm layers stained with the Live/Dead viability kit. As shown in Figure 10B–F, untreated controls were characterized by intact biofilms with predominant viable bacteria (green staining). In contrast, biofilms treated with either ciprofloxacin or AgNP gel showed notable cell death (red staining) and biofilm detachment, indicated by the reduced biofilm thickness. As expected, the number of dead cells increased when treated with AgNPs at the highest dose. We hypothesize that the remarkable capacity of the gel formulation to eliminate established biofilms is due to the ultrasmall size of the AgNPs, which enhances the capacity of AgNPs to disperse the biofilm and kill the bacteria. Hence, this study reports a

https://dx.doi.org/10.1021/acsami.0c09414
ACS Appl. Mater. Interfaces XXXX, XXX, XXX−XXX

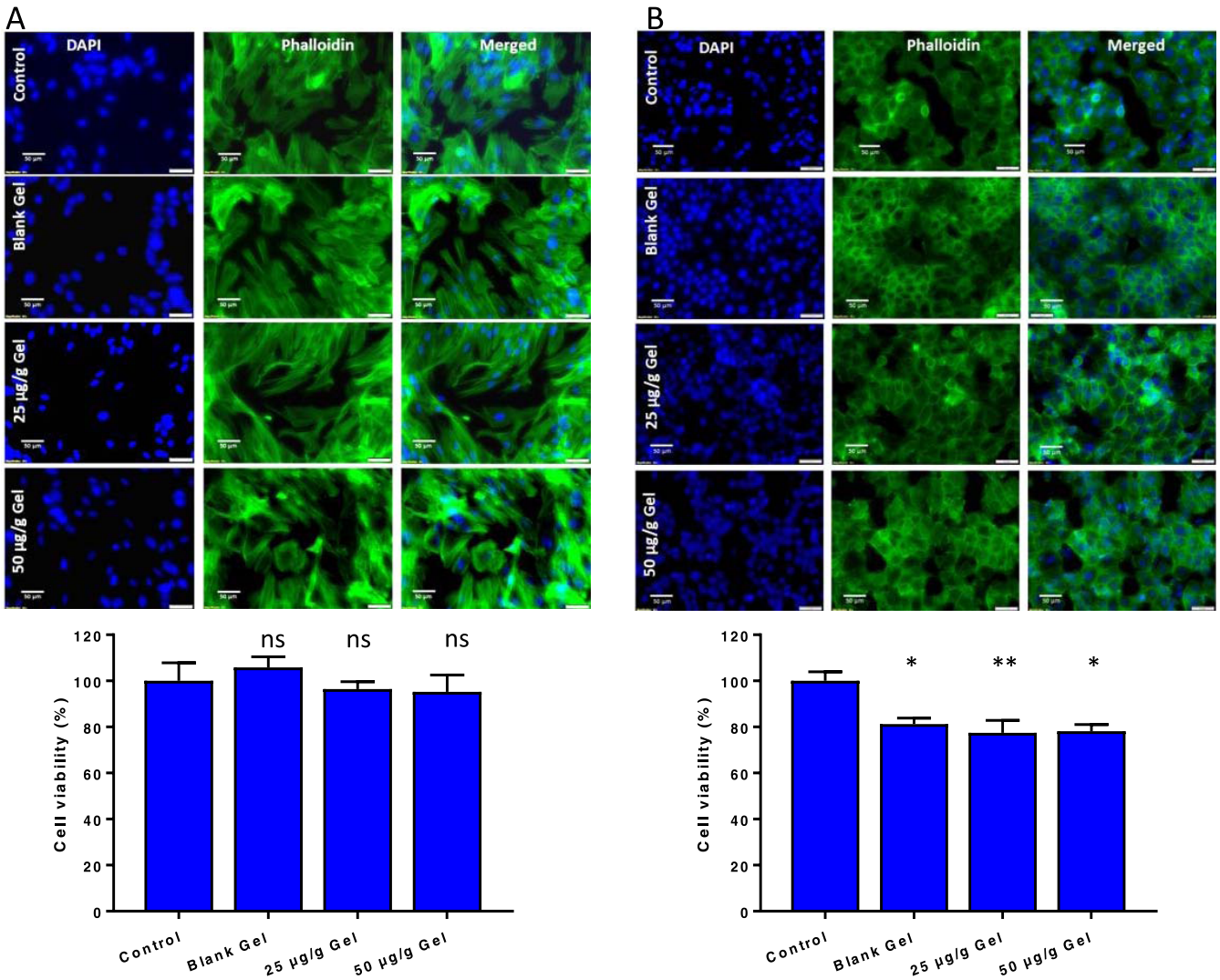

Figure 11. Representative fluorescence microscope images of human foreskin fibroblast (HFF) (A) and HaCaT (B) morphology in the presence or absence of AgNP formulation and their corresponding cell viability after 24 h of exposure. Data are represented as mean ±SD; the * denotes significant difference compared to the control ($P < 0.05$) using one-way ANOVA followed by Dunnett's multiple comparison test, and ns denotes no significance. ns, $P > 0.05$, *$P < 0.05$, **$P < 0.01$, ***$P < 0.001$, and ****$P < 0.0001$.

substantial eradication capacity of this novel formulation against established multispecies biofilms and opens a promising and exciting new avenue in controlling bacterial biofilms, which could improve clinical practice and treatment and management of patients suffering from infected chronic wounds.

Evaluation of Cellular Morphology and Cytotoxicity. In addition to the excellent antibacterial capacity, it is important to evaluate the possible toxicity of the developed hydrogel on human cells. We selected primary human foreskin fibroblasts (HFFs) and human keratinocytes (HaCaTs) as these are the main cell types found in the wound-healing process. As shown in Figure 11A,B, the most effective antibacterial hydrogel containing 50 μg/g AgNPs showed no obvious cytotoxicity to both cell types within 24 h, very similar to the untreated control. The viability of both cells types was found to be above 80%, which is considered as nontoxic according to the International Standard ISO 2009 "Biological evaluation of medical devices".[58] The increased viability observed here could be explained by the higher tolerance of mammalian cells to silver compared to bacteria indicated in other published studies.[59]

The cytocompatibility of the AgNP hydrogel formulation was further confirmed by studying its effects on the cell morphology by assessing the cytoskeletal actin structure to determine whether AgNPs induce changes in the morphology and adhesion of the cells. Fluorescent images of both HaCaTs and HFFs demonstrated no significant changes in the cell morphology and the associated actin cytoskeletal structure (Figure 11A,B). Notably, treated cells appeared healthy and comparable to the untreated controls. This suggests a high level of biocompatibility of the AgNP Pluronic hydrogel with human skin cells even after exposure greater than 24 h. Taken together, the antibacterial hydrogel developed in this study revealed a considerable antimicrobial activity against a broad spectrum of bacteria, including established multispecies biofilms, accompanied by minimal cytotoxicity to mammalian cells *in vitro*. These results offer great promise for future applications of the developed hydrogel using *in vivo* studies to investigate clinically relevant infected wounds. Hence, forthcoming work will focus on preclinical studies in small- and

https://dx.doi.org/10.1021/acsami.0c09414
ACS Appl. Mater. Interfaces XXXX, XXX, XXX−XXX

large-animal models of wound infection and in-depth mechanistic interrogation of the antibacterial potency of the composition.

CONCLUSIONS

We have developed a novel thermosensitive hydrogel composition loaded with ultrasmall AgNPs, which provide a continuous release of silver ions for periods longer than 24 h. The gel has very high efficacy against clinically significant Gram-negative and Gram-positive bacteria. Importantly, we found that the gel has the capacity to disrupt and eradicate established biofilms composed of not only single bacterial species but also multispecies pathogens. Biocompatibility studies using human foreskin fibroblasts and human keratinocytes showed no apparent (or clinically relevant <20%) toxicity to skin cells, which play a critical role in wound healing and tissue regeneration. The potent antibacterial activity of the gel developed in this study could be largely attributed to well-dispersed ultrasmall AgNPs in a complex hydrogel framework that facilitates the continuous and sustained release of silver ions from the hydrogel, hence providing an enhanced capacity to interact with the bacterial membranes and causing significant bacterial cell damage and death. The results presented here open exciting avenues for creating advanced wound management products with superior antibacterial performance, which then could become an effective therapeutic option for difficult-to-treat infected wounds.

ASSOCIATED CONTENT

Supporting Information

The Supporting Information is available free of charge at https://pubs.acs.org/doi/10.1021/acsami.0c09414.

Pluronic F-127 hydrogel formulation composition; DLS and UV−vis spectroscopy of AgNP formulation on days 0, 7, 30, and 60; representative images of a zone of inhibition of AgNPs (25 μg/g); intracellular reactive oxygen species generation in *P. aeruginosa* after exposure to AgNP formulation and H_2O_2 (PDF)

AUTHOR INFORMATION

Corresponding Authors

Nirmal Goswami − *Academic Unit of STEM, University of South Australia, Mawson Lakes, SA 5095, Australia; Materials Chemistry Department, CSIR-Institute of Minerals and Materials Technology, Bhubaneswar 751013, India;* orcid.org/0000-0002-8950-6459; Phone: +91-9330-897 344; Email: ngoswami@immt.res.in

Krasimir Vasilev − *Future Industries Institute and Academic Unit of STEM, University of South Australia, Mawson Lakes, SA 5095, Australia;* orcid.org/0000-0003-3534-4754; Phone: +61 8 830 25697; Email: Krasimir.vasilev@unisa.edu.au

Authors

Hanif Haidari − *UniSA Clinical & Health Sciences and Future Industries Institute, University of South Australia, Adelaide, SA 5000, Australia*

Zlatko Kopecki − *UniSA Clinical & Health Sciences and Future Industries Institute, University of South Australia, Adelaide, SA 5000, Australia*

Richard Bright − *Academic Unit of STEM, University of South Australia, Mawson Lakes, SA 5095, Australia*

Allison J. Cowin − *UniSA Clinical & Health Sciences and Future Industries Institute, University of South Australia, Adelaide, SA 5000, Australia;* orcid.org/0000-0003-2885-2080

Sanjay Garg − *UniSA Clinical & Health Sciences, University of South Australia, Adelaide, SA 5000, Australia*

Complete contact information is available at: https://pubs.acs.org/10.1021/acsami.0c09414

Author Contributions

The manuscript was written through the contributions of all authors. All authors have approved the final version of the manuscript.

Notes

The authors declare no competing financial interest.

ACKNOWLEDGMENTS

K.V. thanks ARC for DP15104212, NHMRC for fellowship APP1122825, and Project grant APP1032738 and the Alexander von Humboldt Foundation for Fellowship for Experienced Researchers. A.J.C. is supported by the NHMRC Senior Research Fellowship (GNT #1102617). Z.K. is supported by the University of South Australia Future Industries Institute Foundation Fellowship and DEBRA Australia Research Grant.

ABBREVIATIONS

MSA, mercaptosuccinic acid
AgNPs, silver nanoparticles
CFU, colony-forming units
CLSM, confocal laser scanning microscopy
CV, crystal violet
DAPI, diamido-2 phenyllindole dihydrochloride
DCFH-DA, 2′,7′-dichlorofluorescin diacetate
DLS, dynamic light scattering
DMEM, Dulbecco's modified Eagle's medium
EDS, energy-dispersive X-ray spectrometry
HaCaTs, human keratinocytes
HFFs, human foreskin fibroblasts
HMDS, hexamethyldisilazane
PF-127, pluronic F-127
PG, propylene glycol
P. aeruginosa, *Pseudomonas aeruginosa*
ROS, reactive oxygen species

REFERENCES

(1) Podolsky, S. H. The evolving response to antibiotic resistance (1945−2018). *Palgrave Commun.* **2018**, *4*, 1−8.
(2) Barriere, S. L. Clinical, economic and societal impact of antibiotic resistance. *Expert Opin. Pharmacother.* **2015**, *16*, 151−153.
(3) O'Neill, J. Antimicrobial Resistance: Tackling a Crisis for the Health and Wealth of Nations (London). Review on Antimicrobial Resistance, 2014.
(4) Chowdhury, N. R.; MacGregor-Ramiasa, M.; Zilm, P.; Majewski, P.; Vasilev, K. 'Chocolate' silver nanoparticles: Synthesis, antibacterial activity and cytotoxicity. *J. Colloid Interface Sci.* **2016**, *482*, 151−158.
(5) Wu, J.; Li, F.; Hu, X.; Lu, J.; Sun, X.; Gao, J.; Ling, D. Responsive Assembly of Silver Nanoclusters with a Biofilm Locally Amplified Bactericidal Effect to Enhance Treatments against Multi-Drug-Resistant Bacterial Infections. *ACS Cent. Sci.* **2019**, *5*, 1366−1376.

(6) Chen, H.; Wubbolts, R. W.; Haagsman, H. P.; Veldhuizen, E. J. A. Inhibition and Eradication of *Pseudomonas aeruginosa* Biofilms by Host Defence Peptides. *Sci. Rep.* **2018**, *8*, No. 10446.
(7) Wu, H.; Moser, C.; Wang, H.-Z.; Høiby, N.; Song, Z.-J. Strategies for combating bacterial biofilm infections. *Int. J. Oral Sci.* **2015**, *7*, 1−7.
(8) García-Astrain, C.; Chen, C.; Burón, M.; Palomares, T.; Eceiza, A.; Fruk, L.; Corcuera, M. Á.; Gabilondo, N. Biocompatible Hydrogel Nanocomposite with Covalently Embedded Silver Nanoparticles. *Biomacromolecules* **2015**, *16*, 1301−1310.
(9) Taheri, S.; Cavallaro, A.; Christo, S. N.; Smith, L. E.; Majewski, P.; Barton, M.; Hayball, J. D.; Vasilev, K. Substrate independent silver nanoparticle based antibacterial coatings. *Biomaterials* **2014**, *35*, 4601−4609.
(10) Koo, H.; Allan, R. N.; Howlin, R. P.; Stoodley, P.; Hall-Stoodley, L. Targeting microbial biofilms: current and prospective therapeutic strategies. *Nat. Rev. Microbiol.* **2017**, *15*, 740−755.
(11) Flemming, H.-C.; Wingender, J.; Szewzyk, U.; Steinberg, P.; Rice, S. A.; Kjelleberg, S. Biofilms: an emergent form of bacterial life. *Nat. Rev. Microbiol.* **2016**, *14*, 563−575.
(12) Yang, L.; Liu, Y.; Wu, H.; Høiby, N.; Molin, S.; Song, Z. J. Current understanding of multi-species biofilms. *Int. J. Oral Sci.* **2011**, *3*, 74−81.
(13) Burmølle, M.; Webb, J. S.; Rao, D.; Hansen, L. H.; Sørensen, S. J.; Kjelleberg, S. Enhanced Biofilm Formation and Increased Resistance to Antimicrobial Agents and Bacterial Invasion Are Caused by Synergistic Interactions in Multispecies Biofilms. *Appl. Environ. Microbiol.* **2006**, *72*, 3916−3923.
(14) Liu, W.; Jacquiod, S.; Brejnrod, A.; Russel, J.; Burmølle, M.; Sørensen, S. J. Deciphering links between bacterial interactions and spatial organization in multispecies biofilms. *ISME J.* **2019**, *13*, 3054−3066.
(15) Stewart, E. J.; Payne, D. E.; Ma, T. M.; VanEpps, J. S.; Boles, B. R.; Younger, J. G.; Solomon, M. J. Effect of Antimicrobial and Physical Treatments on Growth of Multispecies Staphylococcal Biofilms. *Appl. Environ. Microbiol.* **2017**, *83*, e03483−e03499.
(16) Yuan, X.; Setyawati, M. I.; Leong, D. T.; Xie, J. Ultrasmall Ag +-rich nanoclusters as highly efficient nanoreservoirs for bacterial killing. *Nano Res.* **2014**, *7*, 301−307.
(17) Goreham, R. V.; Mierczynska, A.; Pierce, M.; Short, R. D.; Taheri, S.; Bachhuka, A.; Cavallaro, A.; Smith, L. E.; Vasilev, K. A substrate independent approach for generation of surface gradients. *Thin Solid Films* **2013**, *528*, 106−110.
(18) Tian, Y.; Qi, J.; Zhang, W.; Cai, Q.; Jiang, X. Facile, One-Pot Synthesis, and Antibacterial Activity of Mesoporous Silica Nanoparticles Decorated with Well-Dispersed Silver Nanoparticles. *ACS Appl. Mater. Interfaces* **2014**, *6*, 12038−12045.
(19) Rai, M.; Yadav, A.; Gade, A. Silver nanoparticles as a new generation of antimicrobials. *Biotechnol. Adv.* **2009**, *27*, 76−83.
(20) Haidari, H.; Goswami, N.; Bright, R.; Kopecki, Z.; Cowin, A. J.; Garg, S.; Vasilev, K. The interplay between size and valence state on the antibacterial activity of sub-10 nm silver nanoparticles. *Nanoscale Adv.* **2019**, *1*, 2365−2371.
(21) Zheng, K.; Setyawati, M. I.; Leong, D. T.; Xie, J. Antimicrobial silver nanomaterials. *Coord. Chem. Rev.* **2018**, *357*, 1−17.
(22) Liu, Y.; Lu, W.-L.; Wang, J.-C.; Zhang, X.; Zhang, H.; Wang, X.-Q.; Zhou, T.-Y.; Zhang, Q. Controlled delivery of recombinant hirudin based on thermo-sensitive Pluronic F127 hydrogel for subcutaneous administration: In vitro and in vivo characterization. *J. Controlled Release* **2007**, *117*, 387−395.
(23) Shachaf, Y.; Gonen-Wadmany, M.; Seliktar, D. The biocompatibility of PluronicF127 fibrinogen-based hydrogels. *Biomaterials* **2010**, *31*, 2836−2847.
(24) Elluru, M.; Ma, H.; Hadjiargyrou, M.; Hsiao, B. S.; Chu, B. Synthesis and characterization of biocompatible hydrogel using Pluronics-based block copolymers. *Polymer* **2013**, *54*, 2088−2095.
(25) Ruel-Gariépy, E.; Leroux, J.-C. In situ-forming hydrogels—review of temperature-sensitive systems. *Eur. J. Pharm. Biopharm.* **2004**, *58*, 409−426.
(26) Bhattarai, N.; Ramay, H. R.; Gunn, J.; Matsen, F. A.; Zhang, M. PEG-grafted chitosan as an injectable thermosensitive hydrogel for sustained protein release. *J. Controlled Release* **2005**, *103*, 609−624.
(27) Haidari, H.; Zhang, Q.; Melville, E.; Kopecki, Z.; Song, Y.; Cowin, A. J.; Garg, S. Development of Topical Delivery Systems for Flightless Neutralizing Antibody. *J. Pharm. Sci.* **2017**, *106*, 1795−1804.
(28) Thet, N. T.; Alves, D. R.; Bean, J. E.; Booth, S.; Nzakizwanayo, J.; Young, A. E. R.; Jones, B. V.; Jenkins, A. T. A. Prototype Development of the Intelligent Hydrogel Wound Dressing and Its Efficacy in the Detection of Model Pathogenic Wound Biofilms. *ACS Appl. Mater. Interfaces* **2016**, *8*, 14909−14919.
(29) Bhargava, A.; Pareek, V.; Roy Choudhury, S.; Panwar, J.; Karmakar, S. Superior Bactericidal Efficacy of Fucose-Functionalized Silver Nanoparticles against *Pseudomonas aeruginosa* PAO1 and Prevention of Its Colonization on Urinary Catheters. *ACS Appl. Mater. Interfaces* **2018**, *10*, 29325−29337.
(30) Su, H.-L.; Chou, C.-C.; Hung, D.-J.; Lin, S.-H.; Pao, I. C.; Lin, J.-H.; Huang, F.-L.; Dong, R.-X.; Lin, J.-J. The disruption of bacterial membrane integrity through ROS generation induced by nanohybrids of silver and clay. *Biomaterials* **2009**, *30*, 5979−5987.
(31) Regiel-Futyra, A.; Kus-Liśkiewicz, M.; Sebastian, V.; Irusta, S.; Arruebo, M.; Kyzioł, A.; Stochel, G. Development of noncytotoxic silver−chitosan nanocomposites for efficient control of biofilm forming microbes. *RSC Adv.* **2017**, *7*, 52398−52413.
(32) Kopecki, Z.; O'Neill, G. M.; Arkell, R. M.; Cowin, A. J. Regulation of Focal Adhesions by Flightless I Involves Inhibition of Paxillin Phosphorylation via a Rac1-Dependent Pathway. *J. Invest. Dermatol.* **2011**, *131*, 1450−1459.
(33) Yuan, X.; Setyawati, M. I.; Tan, A. S.; Ong, C. N.; Leong, D. T.; Xie, J. Highly luminescent silver nanoclusters with tunable emissions: cyclic reduction−decomposition synthesis and antimicrobial properties. *NPG Asia Mater.* **2013**, *5*, No. e39.
(34) Li, J.; Mooney, D. J. Designing hydrogels for controlled drug delivery. *Nat. Rev. Mater.* **2016**, *1*, No. 16071.
(35) Hokett, S. D.; Cuenin, M. F.; O'Neal, R. B.; Brennan, W. A.; Strong, S. L.; Runner, R. R.; McPherson, J. C.; Van Dyke, T. E. Pluronic Polyol Effects on Human Gingival Fibroblast Attachment and Growth. *J. Periodontol.* **2000**, *71*, 803−809.
(36) Sood, N.; Bhardwaj, A.; Mehta, S.; Mehta, A. Stimuli-responsive hydrogels in drug delivery and tissue engineering. *Drug Delivery* **2016**, *23*, 748−770.
(37) Ivanova, R.; Lindman, B.; Alexandridis, P. Evolution in Structural Polymorphism of Pluronic F127 Poly(ethylene oxide)−Poly(propylene oxide) Block Copolymer in Ternary Systems with Water and Pharmaceutically Acceptable Organic Solvents: From "Glycols" to "Oils". *Langmuir* **2000**, *16*, 9058−9069.
(38) Islam, M. T.; Rodríguez-Hornedo, N.; Ciotti, S.; Ackermann, C. Rheological Characterization of Topical Carbomer Gels Neutralized to Different pH. *Pharm. Res.* **2004**, *21*, 1192−1199.
(39) Uman, S.; Dhand, A.; Burdick, J. A. Recent advances in shear-thinning and self-healing hydrogels for biomedical applications. *J. Appl. Polym. Sci.* **2020**, *137*, No. 48668.
(40) Tang, Y.-F.; Du, Y.-M.; Hu, X.-W.; Shi, X.-W.; Kennedy, J. F. Rheological characterisation of a novel thermosensitive chitosan/poly(vinyl alcohol) blend hydrogel. *Carbohydr. Polym.* **2007**, *67*, 491−499.
(41) Afinjuomo, F.; Fouladian, P.; Parikh, A.; Barclay, T. G.; Song, Y.; Garg, S. Preparation and Characterization of Oxidized Inulin Hydrogel for Controlled Drug Delivery. *Pharmaceutics* **2019**, *11*, 356−377.
(42) Dai, X.; Zhang, Y.; Gao, L.; Bai, T.; Wang, W.; Cui, Y.; Liu, W. A Mechanically Strong, Highly Stable, Thermoplastic, and Self-Healable Supramolecular Polymer Hydrogel. *Adv. Mater.* **2015**, *27*, 3566−3571.
(43) Rolim, W. R.; Pelegrino, M. T.; de Araújo Lima, B.; Ferraz, L. S.; Costa, F. N.; Bernardes, J. S.; Rodigues, T.; Brocchi, M.; Seabra, A. B. Green tea extract mediated biogenic synthesis of silver nano-

https://dx.doi.org/10.1021/acsami.0c09414
ACS Appl. Mater. Interfaces XXXX, XXX, XXX−XXX

particles: Characterization, cytotoxicity evaluation and antibacterial activity. *Appl. Surf. Sci.* **2019**, *463*, 66−74.
(44) Liu, X.; Gan, H.; Hu, C.; Sun, W.; Zhu, X.; Meng, Z.; Gu, R.; Wu, Z.; Dou, G. Silver sulfadiazine nanosuspension-loaded thermosensitive hydrogel as a topical antibacterial agent. *Int. J. Nanomed.* **2019**, *14*, 289−300.
(45) Le Ouay, B.; Stellacci, F. Antibacterial activity of silver nanoparticles: A surface science insight. *Nano Today* **2015**, *10*, 339−354.
(46) Richter, K.; Facal, P.; Thomas, N.; Vandecandelaere, I.; Ramezanpour, M.; Cooksley, C.; Prestidge, C. A.; Coenye, T.; Wormald, P.-J.; Vreugde, S. Taking the Silver Bullet Colloidal Silver Particles for the Topical Treatment of Biofilm-Related Infections. *ACS Appl. Mater. Interfaces* **2017**, *9*, 21631−21638.
(47) Bjarnsholt, T. The role of bacterial biofilms in chronic infections. *APMIS, Suppl.* **2013**, *121*, 1−58.
(48) Liu, J.; Li, S.; Fang, Y.; Zhu, Z. Boosting antibacterial activity with mesoporous silica nanoparticles supported silver nanoclusters. *J. Colloid Interface Sci.* **2019**, *555*, 470−479.
(49) McShan, D.; Ray, P. C.; Yu, H. Molecular Toxicity Mechanism of Nanosilver. *J. Food Drug Anal.* **2014**, *22*, 116−127.
(50) Choi, O.; Hu, Z. Size Dependent and Reactive Oxygen Species Related Nanosilver Toxicity to Nitrifying Bacteria. *Environ. Sci. Technol.* **2008**, *42*, 4583−4588.
(51) Jin, J.-C.; Wu, X.-J.; Xu, J.; Wang, B.-B.; Jiang, F.-L.; Liu, Y. Ultrasmall silver nanoclusters: Highly efficient antibacterial activity and their mechanisms. *Biomater. Sci.* **2017**, *5*, 247−257.
(52) Zhang, L.; Wu, L.; Si, Y.; Shu, K. Size-dependent cytotoxicity of silver nanoparticles to Azotobacter vinelandii: Growth inhibition, cell injury, oxidative stress and internalization. *PLoS One* **2018**, *13*, No. e0209020.
(53) Morones, J. R.; Jose Luis, E.; Alejandra, C.; Katherine, H.; Juan, B. K.; Jose Tapia, R.; Miguel Jose, Y. The bactericidal effect of silver nanoparticles. *Nanotechnology* **2005**, *16*, 2346−2353.
(54) Burd, A.; Kwok, C. H.; Hung, S. C.; Gu, H.; Hua, G.; Lam, W. K.; Huang, L. A comparative study of the cytotoxicity of silver-based dressings in monolayer cell, tissue explant, and animal models. *Wound Repair Regen.* **2007**, *15*, 94−104.
(55) Alvarado-Gomez, E.; Martínez-Castañon, G.; Sanchez-Sanchez, R.; Ganem-Rondero, A.; Yacaman, M. J.; Martinez-Gutierrez, F. Evaluation of anti-biofilm and cytotoxic effect of a gel formulation with Pluronic F-127 and silver nanoparticles as a potential treatment for skin wounds. *Mater. Sci. Eng., C* **2018**, *92*, 621−630.
(56) Dosler, S.; Karaaslan, E. Inhibition and destruction of *Pseudomonas aeruginosa* biofilms by antibiotics and antimicrobial peptides. *Peptides* **2014**, *62*, 32−37.
(57) Fang, K.; Jin, X.; Hong, S. H. Probiotic *Escherichia coli* inhibits biofilm formation of pathogenic *E. coli* via extracellular activity of DegP. *Sci. Rep.* **2018**, *8*, No. 592.
(58) ISO, I.S.. Biological Evaluation of Medical Devices. *Part 5: Tests for In Vitro Cytotoxicity*; ISO: Switzerland, 2009.
(59) Vasilev, K.; Sah, V.; Anselme, K.; Ndi, C.; Mateescu, M.; Dollmann, B.; Martinek, P.; Ys, H.; Ploux, L.; Griesser, H. J. Tunable antibacterial coatings that support mammalian cell growth. *Nano Lett.* **2010**, *10*, 202−207.

https://dx.doi.org/10.1021/acsami.0c09414
ACS Appl. Mater. Interfaces XXXX, XXX, XXX−XXX